Flight Paths

Related terms:

Neutron Source, Electrons, Fission, Flight Time, Spectrometers, Neutrons, Diffractometers, Photons, Gamma Radiation, Ion

View all Topics

Aircraft Performance and Design

Francis Joseph Hale, in Encyclopedia of Physical Science and Technology (Third Edition), 2003

I Aircraft Flight Behavior

The flight path and behavior of an aircraft are determined by the interaction between the characteristics of the aircraft and the environment in which it is flying. The aircraft characteristics can be categorized as the physical characteristics, such as the shape, mass, volume, and surface area; the characteristics of the subsystems, such as the propulsion, guidance, and control systems; and the structural characteristics, such as loading and temperature limitations and the stiffness (rigidity) of the structure.

The environment affects the flight of an aircraft through the field forces and the surface forces. The only field force that need be considered is gravity, which appears as the weight and is a function of the mass. The surface forces are the aerodynamic forces (the lift, the drag, and the side force) which are strongly dependent on the shape and surface area of the aircraft, especially of the wings; the properties of the atmosphere; and the airspeed. In addition, consideration must be given to the inertial forces, which are a consequence of nonequilibrium processes and maneuvers and which play an important role in the dynamic and stress analyses of aircraft but not in performance analyses; inertial forces are ignored in this article.

Although most modern aircraft have various amounts of elasticity arising from the desire to reduce the structural weight to a minimum, aeroelastic effects need not be considered in initial performance analyses and preliminary configuration designs. Furthermore, the three rotational modes of a rigid aircraft can be ignored

by considering the aircraft to be a point mass, and the inertia forces can be neglected (with the exception of the centrifugal force in turning flight) by assuming that velocities and other flight-path parameters are either constant or changing so slowly that their rates of change can be neglected. However, an acceleration correction should be made for the climb of a high-performance aircraft.

With the assumptions and approximations of the preceding paragraphs, the performance problem can be reduced to a set of simple, two-dimensional statics problems that, although idealized and not applicable to all classes of aircraft or flight regimes, are amazingly powerful in providing insight into the reasons that conventional aircraft look and fly as they do. It is interesting to discover that turbojet aircraft fly high and fast not necessarily because they want to but because they must do so if they are to be competitive with piston–propeller aircraft.

> Read full chapter

Molecular Physics

Ruslan P. Ozerov, Anatoli A. Vorobyev, in Physics for Chemists, 2007

EXAMPLE E3.15

A free path flight □ of CO_2 gas at normal conditions is □ = 40 nm. Determine the molecule's average speed «□» and the number of impacts *z* a molecule undergoes in 1 sec.

Solution: The average molecule speed can be found according to expression (3.3.7□). Substituting the known and given values we obtain «□» = 362 m/sec. The average number of impacts can be found according to equation *z* = □/□ (the averaging sign is omitted here). Substituting the given values in this equation, we arrive at $z = 9.05 \times 10^9$ sec^{-1}.

> Read full chapter

Sector Mass Spectrometers*

R. Bateman, in Encyclopedia of Spectroscopy and Spectrometry (Second Edition), 1999

Single-Focusing Magnetic Sector

If a parent ion fragments in the flight path between the source and the magnetic field, or the 'first field-free region', the daughter ion has an energy relative to that of the parent in proportion to the ratio of their masses (m_d/m_p). Ions originating in the ion source are accelerated to the same kinetic energy. Consequently, after traversing the magnetic sector, the daughter ion appears at a different mass (m^*) when viewed relative to the normal spectrum. The apparent mass is given by:

[10]

The daughter ion peak is often recognizable since it is usually broader as a result of its increased energy spread. The parent and daughter ions can often be deduced from m^* with reasonable confidence if the sample is pure, but not if a mixture. This can provide useful additional information or become a source of noise depending on the circumstances.

> Read full chapter

Aircraft Avionics

Robert G. Loewy, in Encyclopedia of Physical Science and Technology (Third Edition), 2003

III.G Collision Avoidance Systems

Although ground control of aircraft flight plans and flight paths in real time have as a prime objective eliminating the possibility of mid-air collisions, controlled flight into terrain, or collisions on airport taxiways or runways, vehicle borne avionics equipment plays important roles in these functions. Installation of airborne, mid-air collision systems provides protection against such calamities independent of ground control and in addition to the nation's Air Traffic Control (ATC) system. The Traffic Alert and Collision Avoidance System (TCAS) uses a scanning radar transmitter in one aircraft to trigger the response of a transponder in any aircraft so equipped within its range. In the version of TCAS most used, TCAS II, the distance between two aircraft and their altitude separation are calculated, based on the transponder signal returns, and the crew is alerted about 40 sec before the closest Point of Approach (CPA) is to be reached, if the separation is predicted to be small. This alert is known as a "traffic advisory" and displays the range, bearing and altitude of the aircraft posing collision danger. If the danger continues, about 25 sec before CPA, a "Resolution Advisory" (RA) appears showing the climb or descent maneuver recommended to increase the miss distance. Since both TCAS-equipped aircraft must be properly advised as to how to change their flight paths, TCAS II has an air-to-air data link

communicating between the two aircraft, to coordinate RA's. A version known as TCAS I does all of this except displaying RA's. All air carrier aircraft operating in U.S. airspace with 10 to 30 passenger seats must have TCAS I, all with more than 30 seats must have TCAS II.

As air travel departure and arrivals increase and, with them, airport congestion, the danger of collision between aircraft on the ground also increases. Ground-based systems to aid the regulation of ground movement of aircraft include surface movement radars and taxiway lights modulated to indicate specific taxi routes. These don't, at this writing, require avionics equipment on the aircraft. There are, however, aircraft systems that use transponders to allow ground-based “interrogators,” located with taxiway lights, to derive identification and location information and relay it to tower controllers.

Commercial, in fact all civil, aviation must keep a safe altitude above terrain in all flight modes other than take-off and landing. Military aircraft, however, must often approach the ground for weapon delivery, precise reconnaissance, or—for extended flight times—to avoid detection or defensive weapons. Those with the last of these requirements are usually equipped with “terrain following” equipment. These are automatic systems having Forward Looking radars and Infra-Red (FLIR) sensors and radar altimeters (see Section III.I, below). The first two of these measure the range and angle from the horizontal of the terrain before the aircraft. Flight path control commands, based on a computed terrain profile in a vertical plane, based on the forward-looking radar returns with pilot monitoring, directly control the pitch attitude, hence “angle of attack” and lift of the aircraft, so as to maintain a desired height above the terrain. The radar altimeter checks the altitude prediction, and the FLIR provides back-up data to ensure that the radar commands flight over such obstructions as power lines. In civil aviation, Controlled Flight Into Terrain (CFIT) has become a safety issue of increasing concern, particularly in mountainous regions and under conditions of reduced visibility. Appropriate avionics therefore, may soon be appearing on all aircraft above a certain size in terrain avoidance applications.

> Read full chapter

DEVELOPMENT OF A HIGH-SPEED, REPETITIVE PELLET LAUNCHER FOR JET

J. LAFFERANDERIE, ... K. SONNENBERG, in Fusion Technology 1990, 1991

4 SABOT DEFLECTION

We are mainly developing two methods for separating the sabot from the pellet flight path.

- One method uses a split sabot which is put into rotation in the barrel. A rifled barrel has been produced with two diametrally opposed helicoidal (n = 1 turn/m), 0.6 mm deep, 1.8 mm wide rifles. The barrel length is 1.3 m. The sabot (fig. 4) is made with lateral fins to be guided by the rifles during acceleration. The rotation speed is limited by the stress induced at the pellet center.

(V_p = pellet velocity). Taking $\sigma \leq 5$ kg/cm^2, $\rho = 0.2$ g/cm^3, r = 0.27 cm, n = 1 turn/m, we find : $V_p \leq 4500$ m/s.

The theoretical radial deviation of the centers of mass of each half of the sabot is :

It is half when velocities close to 10 km/s are considered due to lower values of n imposed by the stress limitation. Preliminary tests have been made at pellet velocities ≤ 3 km/s. In order to increase r_G, the sabots are made in asymetrical way. Fig. 7 shows the impacts of three successive pellets on a target, 4 m far from the barrel muzzle. The distance between ice and most of sabot pieces is ≥ 3 cm. Sometimes, we get a small impact at 1 or 2 cm from the pellet, which we think to be due either to a piece of ice or to a sabot part having interacted with the vacuum enclosure walls. The pellet angular scattering is small (pellet impacts inside a 16 mm diameter circle).

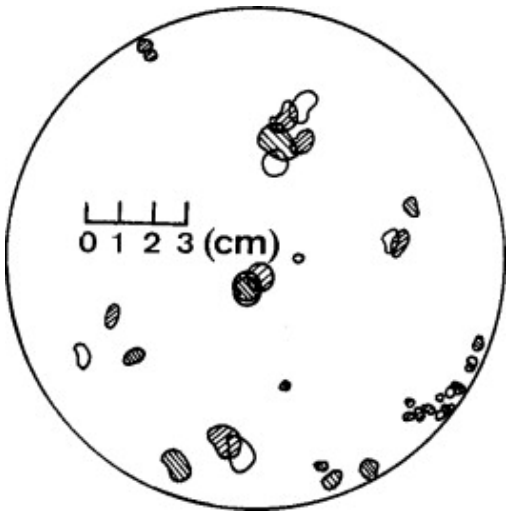

FIGURE 7. Impacts of 3 successive pellets on a target, 4 m far from the barrel muzzle

- A second method uses a single sabot inside a linearly rifled barrel. Tests have shown it is possible to get an axial separation between the sabot and the pellet inside the barrel by using a sufficiently long barrel, because friction forces become higher than the driving force and decelerate the sabot without decelerating the pellet. The end part of the barrel is slightly incurved as a “ski-jump”. The sabot being guided by the rifles follows the curvature as the pellet keeps its linear trajectory. The resulting deflection is :

(L = length of the curved part of the barrel, R = radius of curvature), which gives

when L = 10 cm and R = 5 m.

A barrel has been ordered which will allow to test this proposal.

> Read full chapter

Neutron Scattering – Fundamentals

Masatoshi Arai, in Experimental Methods in the Physical Sciences, 2013

3.8.2.2 Bandwidth Choppers

Pulsed neutron sources produce pulsed neutrons at the accelerator frequency. Neutrons disperse along the flight path according to their different speeds. Slow neutrons reach the detector at a very late time, when faster neutrons from the following time frame can arrive and mix with the slow neutrons, producing a background. Therefore, it is important to eliminate unusable slow neutrons from the early frame and fast neutrons from the late frame. Figure 3.81 shows an example of frame definition by bandwidth choppers. The first chopper near the source eliminates most of unusable neutrons from the reference frame. The second chopper stops neutrons from earlier frames. However, these are not enough to eliminate neutrons from further previous frames, which may go to the sample at nine frames later. These very slow neutrons are negligible in most cases; however, they can produce a serious background for small-angle scattering or reflectivity measurements, where very slow neutrons have a very high scattered intensity or reflectivity. Therefore, in most cases three bandwidth choppers are installed for such instruments. Figure 3.82 shows a bandwidth chopper developed for J-PARC. The absorbing material is B_4C, so that it can stop even epithermal neutrons effectively.

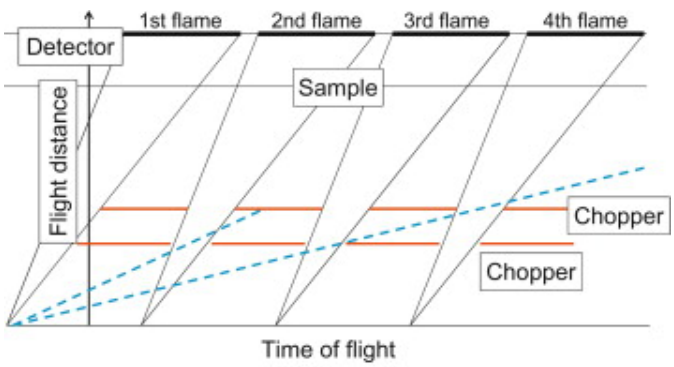

Figure 3.81. Illustrating how bandwidth choppers eliminate neutrons from previous frames.

Figure 3.82. A bandwidth chopper developed at J-PARC.

> Read full chapter

Systematic Synthesis of Monolayer-Protected Gold Clusters with Well-Defined Chemical Compositions

Tatsuya Tsukuda, ... Yuich Negishi, in Metal Nanoclusters in Catalysis and Materials Science, 2008

2.3.3 *TOF Mass Spectrometer*

The cluster ions were counted either by a microchannel plate detector located at the end of the flight path (F4655-10, Hamamatsu) or by that with a center hole (LPD-25, Burle) after reflection by the retarding field of the reflectron. Pulsed signals from the detector were accumulated by a multichannel scaler/averager (SR430, Stanford Research Systems). The data were transferred and stored in a Windows computer using a LABVIEW program. The repetition rate was 130 and 10 Hz for collecting the ESI and LDI mass spectra, respectively. The resolution of the mass spectrometer ($M/\Delta M$), with and without the reflectron, was typically 1000 and 400, respectively. Mass spectra of the ions of either polarity were recorded by changing the polarities of the power supplies. The LDI and ESI mass spectra obtained were calibrated by referencing with those of C_{60} and NaI cluster ions recorded under the same conditions, respectively.

> Read full chapter

Glow Discharge Mass Spectrometry

C. Derrick QuarlesJr, ... R. Kenneth Marcus, in Encyclopedia of Spectroscopy and Spectrometry (Second Edition), 2010

Mass Analysis and Quantification

GD plasmas commonly operate between 0.1 and 10 Torr, whereas MS systems operate at a pressure of ~10^{-5} Torr to prevent the collision of ions during their flight path or arcing due to high voltages. Therefore, the transport of ions from the plasma to the mass analyzers in GDMS instruments involves three vacuum regions: (1) the GD ionization source (~1 Torr), (2) the intermediate region (~10^{-4} Torr), and (3) the mass analyzer region (~10^{-6} Torr). Since the 1970s, GD ion sources have been interfaced to all of the common mass analyzers, including magnetic sectors, quadrupole mass filters, quadrupole ion traps, time-of-flight (TOF) devices, and Fourier transform ion cyclotron resonance (FT-ICR) devices. Although the low-pressure GD plasma is sustained in a high-purity (>99.999%) argon discharge gas, there are instances of spectral interferences due to residual gases as well as isobaric elemental overlaps and the presence of dimers and argide species. For this reason, magnetic sector instruments have been by far the predominant analyzers in commercial systems. The first commercially available GDMS system employed a double-focusing analyzer and has been employed successfully for depth profiling and the analysis of metal alloys, semiconductors, powders, and nonconductors (with RF powering) with nominal resolution on the order of 4000 and parts-per-billion-level sensitivities. Another commercially available GDMS was the VG GloQuad (VG Elemental, Thermo group), which employed a quadrupole mass filter. Table 2 includes a comparison of the mass analyzers used in GDMS, and Figure 4 depicts a general schematic diagram of a GD quadrupole mass spectrometer system.

Table 2. Comparison of mass analyzers for GDMS

Mass analyzer	Ion dispersion	Advantages	Disadvantages	Interface to GD
Sectors	Space	• Discriminate isobaric interferences • Commercially available (1980s)	• Complex and costly • Scan speed	1970s
Time-of-flight	Time	• Simple • Speed • Good resolution with reflection	• Complicated ion extraction	1990s
Quadrople mass filter	Selective m/z transmission	• Scan speed	• Limited resolution	1970s

		• Peak hopping • Commercially available • Compact design • Low cost in comparison to magnetic sectors		
Ion trap	Selective m/z ejection	• Remove polyatomic isobaric interferences using CID • Compact design • Less expensive than quadrupoles and magnetic sectors	• Ion admission from external sources	1990s
FT-ICR	Magnetic trapping and cyclotron frequency measurement	• High resolution resolves isobaric interferences • CID possible for the removal of polyatomic interferences	• Cost and complex • Limited dynamic range because of space charging effects • Ion admission from external sources	1980s

Note: CID, collision-induced dissociation.

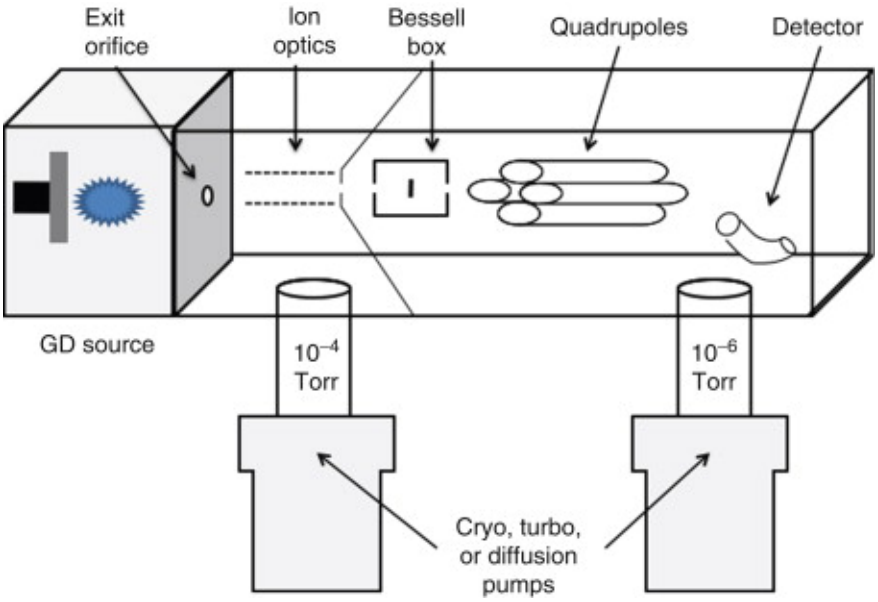

Figure 4. General schematic diagram of a GD quadrupole mass spectrometer.

GD source interfacing to OES and MS instruments has been undertaken for the elemental analysis of bulk solid materials, as well as for depth profiling. The mass spectra obtained by GDMS allow for more simplistic interpretation of qualitative results when compared to the emission spectra because each element has fewer isotopes than optical transitions. Calibration curves and relative sensitivity factors (RSFs) are the two most common quantification methods used in GDMS, although well-defined calibration standards or reference materials are required as opposed

to simple generation of calibration curves based on serial dilution of standard solutions. The experimental factors taken into account when performing any analysis by GDMS are sample (matrix) composition, sample positioning, discharge pressure and power, source configuration, ion sampling efficiency, and mass analyzer.

Use of the calibration curve method can be problematic in GDMS because of the many sources of irreproducibility (e.g., sample position) and the large number of elements targeted in a sample. Despite these facts, Grimm-type sources can provide accurate sample placement and create calibration curves with acceptable variability and linear response when using external standards. Overall, the number of materials available to be used as external standards is insufficient in many applications; therefore, internal standards are a virtual necessity for GDMS analysis. By using internal standards, matrix interferences and signal drift/deviation over time can also be compensated.

The second method used for GDMS quantification, based on the use of RSFs, was first developed for spark source MS. The RSF of an analyte element, x, is the ratio of its sensitivity (intensity, *I*, per unit concentration, *C*) to the sensitivity of some reference element, r:

[1]

During the quantification of an unknown sample, RSFs are applied to the ion beam ratios. The ion beam ratio is the ratio of the isotope's ion current with respect to the total ion current and represents the concentration of that isotope in the sample. For most of the elements across the periodic table, the RSF values are within one order of magnitude of each other and do not vary much between sample matrices that have the same general composition. Because RSFs are effectively based on the relative ionization efficiencies of the elements within a sample, the variations in the materials' sputtering rates do not affect the RSF values. Therefore, GDMS has the ability to perform standardless semiquantitative analysis to achieve accuracies on the order of 20%. When higher accuracy quantitative analysis is required, RSFs based on matrix-matched standards do provide single-digit values.

> Read full chapter

The Stardust sample return mission

Scott A. Sandford, ... Michael E. Zolensky, in Sample Return Missions, 2021

4.3.1.2 Dust flux monitor data

During the flyby the dust detectors recorded particle impacts of masses ranging from 10^{-11} to > 10^{-4} g. The impact distribution along *Stardust's* flight path was extremely non-uniform. Dust impacts occurred in short "bursts" that could contain nearly a thousand particles separated by intervals in which no dust arrived at all (Tuzzolino et al. 2004) (Fig. 4.4). The most likely explanation for this behavior is the ejection of larger particle aggregates from the nucleus that fragmented as they moved out into the coma (Clark et al. 2004). At least seven impacting particles were big enough (the largest □4 mm in diameter) to penetrate the spacecraft's front bumper shield and be detected by the flux monitor's acoustic sensors (Green et al. 2004). These data indicated that the expected samples were successfully collected by the aerogel collector during the flyby.

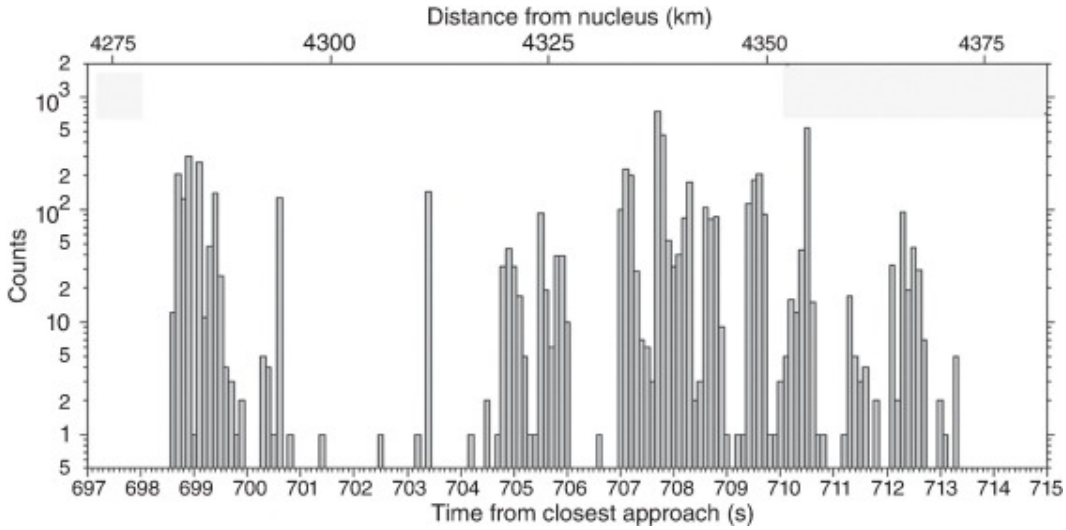

Fig. 4.4. Eighteen seconds of data from the Dust Flux Monitor taken when the spacecraft was ~4300 km from the nucleus of 81P/Wild 2, showing the variable impact rate seen as the spacecraft passed through the comet's coma (adapted from Clark et al. 2004).

> Read full chapter

Neutron Diffraction, Instrumentation

A.C. Hannon, in Encyclopedia of Spectroscopy and Spectrometry, 1999

Resolution of a pulsed source diffractometer

For a time-of-flight diffractometer the three major contributions to the *Q*-resolution are due to the geometrical uncertainty in angle, $\Delta\theta$, the uncertainty in flight path, ΔL, and the uncertainty in time-of-flight, Δt, leading to the following expression for the total combined resolution width:

The angular uncertainty for a time-of-flight diffractometer, $\Delta\theta$, is similar to the reactor case in that it arises from the acceptance angle of the collimation in front of the moderator, the size of the sample and the acceptance angle of the detector. However, there is a major difference in its effect because of the way in which a single detector measures a complete diffraction pattern without moving to different scattering angles, 2θ, so that the angular contribution to $\Delta Q/Q$ is independent of Q. This contribution to the resolution is ideally suited to powder diffraction because it has a Δd which is small for short d-spacing where Bragg peaks are very close together, and only becomes large at high d-spacing where Bragg peaks are well separated.

The flight path uncertainty, ΔL, arises from the finite sizes of the moderator, sample and detector. Its contribution to the resolution is symmetric and may be approximated by a Gaussian, as is also the case for the angular contribution. The contribution to $\Delta d/d$ due to the flight path uncertainty may be minimized simply by using a very long flight path, L, although this may only be achieved at the expense of a corresponding decrease in the count rate.

At low and medium scattering angles, cot θ is relatively large and the angular contribution to the resolution tends to dominate. However, at backward angles ($2\theta \rightarrow 180°$) this contribution becomes very small so that a diffraction pattern can be measured with a very narrow angular resolution across its entire range. The time-of-flight uncertainty, Δt, is then of greater importance. Its main component is the time uncertainty which arises from the moderation process. This gives an exponential contribution to the resolution with a decay time, τ, which is the mean time spent in the moderator for neutrons of a particular wavelength. Figure 14 shows the resolution of the LAD time-of-flight diffractometer at backward angle, obtained by fitting the convolution of a Gaussian and an exponential to Bragg peaks in experimental data. The Gaussian contribution to $\Delta d/d$ is almost independent of d-spacing, as predicted. The detailed behaviour of the decay time, τ, depends upon the design of the moderator, but is generally small at short times (i.e. for high energy neutrons) and tends to a large value at long times (i.e. for low energy neutrons). The overall peak shape, Gaussian-exponential convolution (see inset to Figure 14), has a very sharp leading edge which can be advantageous in resolving overlapping peaks.

Figure 14. The measured experimental resolution of the LAD pulsed neutron diffractometer at backward angle, 2□ = 146°. The total full width at half maximum (FWHM) and the FWHM for the Gaussian contribution are shown in the form of $\Delta d/d$. Also shown is the decay constant □ for the exponential contribution to the resolution. The inset shows the peak shape measured for a typical Bragg peak (the (331) reflection for polycrystalline silicon).

> Read full chapter